JOURNAL OF MATERIALS SCIENCE 21 (1986) 1553–1560

Microstructural characterization of two lithium-containing aluminium alloys

T. S. SRIVATSAN
Georgia Institute of Technology, Altlanta, Georgia 30332, USA
E. J. COYNE Jr
Lockhead-Georgia Company, Marietta, Georgia 30063, USA
E. A. STARKE Jr
Dean of Engineering, University of Virginia, Charlottesville, Virginia 22901, USA

The microstructures of two lithium-containing aluminium alloys have been investigated. The two alloys were an Al–Li–Mn alloy, heat treated to provide an under-aged, peak-aged and an over-aged condition, and a commercial Al–Cu–Li alloy, 2020, heat treated and aged to contain ordered precipitate structures. It was observed that both materials were recrystallized with fairly large grains. The Al–Li–Mn material had a high volume fraction of Al_6Mn dispersoids and the Al–Cu–Li alloy had a substantial volume fraction of coarse intermetallic particles and intermediate size disperoids. The major strengthening precipitates were identified from bright-field and dark-field images and selected-area diffraction patterns taken in the transmission electron microscope. Precipitate-free zones were found to be present in both the Al–Li–Mn and Al–Cu–Li alloys. The results of this study suggest that the peak-aged Al–Cu–Li alloy and the under-aged and peak-aged Al–Li–Mn alloys enhance deformation to occur primarily by planar slip, and the larger particle size and interparticle spacing of the over-aged Al–Li–Mn promotes a combination of planar slip and Orowan looping.

1. Introduction

The aerospace industry continuously examines alternative materials to the most commonly used aluminium alloys. These studies have led to an increased usage of composites. However, composites are difficult to fabricate, involve expensive manufacturing processes and are not always readily available. Fail-safe and safe-life design concepts and an increased emphasis on efficiency and reliability have stimulated the development of new aluminium alloys. These alloys could potentially provide excellent combinations of high strength, fracture toughness, resistance to exfoliation corrosion, resistance to stress corrosion cracking, reduced density, improved thermal stability and better stiffness.

Lithium-containing aluminium alloys are attractive materials for stiffness-critical-airframe-structures due to their high strengths, low densities, high elastic moduli and good corrosion resistance. For lithium additions up to 4 wt %, each weight per cent of lithium reduces the density by 3% and increases the elastic modulus by 6% [1]. The specific modulus (modulus of elasticity/weight) of an alloy with 2.8% lithium by weight is 20% higher than that of alloy 2024–T351 and 26% higher than that of alloy 7075–T651 [2]. The higher specific modulus of these alloys reduces the rate of fatigue crack growth and the decrease in density is effective in reducing structural weight [2]. However, age hardenable lithium-containing aluminium alloys suffer problems associated with low ductility and inadequate fracture toughness caused by strain localization. In these alloys strain localization is caused by the precipitation of fine, uniformly spaced $\delta'(Al_3Li)$ particles in association with precipitate-free zones (PFZs) adjacent to the grain boundaries. In order to overcome this problem, alloy development efforts have been concentrated on the addition of dispersoids to refine the grain size and to minimize strain localization.

This paper presents the results of a systematic characterization of the microstructures of an aluminium alloy containing 3 wt % lithium with manganese added as grain refiner and a commercial Al–Cu–Li alloy, 2020, aged to contain ordered precipitate structures. The paper describes metallographic observations of the grain structure, scanning electron microscopic observations of particle distributions and transmission electron microscopic determinations of the precipitate structures.

2. Precipitation sequence in lithium-containing aluminium alloys

When the aluminium–lithium system is quenched from a single-phase field and subsequently aged in a two-phase field, decomposition of the supersaturated solid solution occurs by the continuous precipitation of coherent δ' (Al_3Li) throughout the matrix. The atomic arrangement of aluminium and lithium atoms in the metastable precipitate is similar to the Ll_2 crystal structure [3]. The metastable precipitate is

0022–2461/86 $03.00 + .12

coherent with the matrix and forms as spheres with a cube/cube orientation relationship with the matrix. The close match of the precipitate and matrix lattice parameters results in a misfit strain of 0.18% [4, 5]. The system has a low interfacial energy which promotes a homogeneous distribution of the coherent precipitate. Heterogeneous precipitation of the equilibrium δ-phase, AlLi, occurs preferentially at planar interfaces, such as grain boundaries. The formation of solution-depleted, relatively weak PFZs is due to the coarsening of this phase [6]. Consequently, plastic deformation is localized in these soft regions resulting in high stress concentrations at grain-boundary triple points. Cracks nucleate at the triple points or at grain-boundary precipitates and propagate intergranularly within the PFZs.

The addition of manganese to aluminium–lithium binary alloys results in the formation of an intermetallic compound Al_6Mn. These incoherent dispersoids help control grain size and shape but are inadequate to totally prevent strain localization in the matrix and PFZs. The Al_6Mn disperoids promote the formation of the equilibrium δ-phase, AlLi, which has a deleterious effect on the corrosion resistance of these alloys [7].

Copper additions of lithium-containing aluminium alloys have been effective in increasing strength. The precipitation sequence for high-copper, low-lithium alloys can be summarized as:

$$\text{supersaturated solid solution} \rightarrow \text{GP zones} \rightarrow \theta'' \rightarrow \theta' \rightarrow \theta \rightarrow T_1$$
$$\text{supersaturated solid solution} \rightarrow \delta' \rightarrow \delta \rightarrow T_1$$

(GP = Guinier–Preston). The lithium and copper follow the sequences established in the aluminium–lithium and aluminium–copper binary alloys, respectively. Ageing at temperatures of commercial importance produces a homogeneous dispersion of θ'' precipitates. A second metastable precipitate, θ', Al_2Cu, forms as thin platelets along the (1 0 0) habit planes. Cadmium, in this alloy system, suppresses the nucleation of θ'' and promotes the formation of θ' [8].

Lithium in the Al–Cu–Li system combines with both aluminium and copper to form a thermodynamically stable, partially coherent phase, T_1, in the peak-aged condition. The T_1 precipitate has a hexagonal crystal structure, an approximate composition of Al_2CuLi, and forms as extremely thin, hexagonal-shaped platelets with a (1 1 1) habit plane. A fine dispersion of T_1 provides adequate strengthening in the peak-aged condition. Depending on the degree of supersaturation, the nucleation of the T_1 phase occurs at GP zones or at dissociated dislocations by a stacking-fault mechanism [9]. In the peak-aged condition, the remaining lithium combines with aluminium to form the binary phase, δ' (Al_3Li). Other precipitates to form in the Al–Cu–Li system of interest are T_B ($Al_{15}Cu_8Li_2$) and T_2 (Al_6CuLi_3). In leaner aluminium alloys, such as 2020, precipitates P, Q and R (Al_5CuLi_3) are formed. The structure of precipitates T_2, P, Q and R and the compositions of P and Q have not yet been determined. The T_B phase has a CaF_2-type cubic structure and forms from the metastable precipitate θ' by the replacement of aluminium atoms with lithium. The T_2 phase was found to occur in lithium-containing aluminium alloys in the shape of massive rounded particles [10].

TABLE I Alloy compositions (wt %)

Alloy	Li	Cu	Si	Fe	Zn	Ti	Cd	Mn*	Al
Al–Li–Mn	3.0	0	0.05	0.05	–	–	–	1.25	bal.
Al–Cu–Li	1.21	4.45	0.08	0.16	0.04	0.06	0.21	0.51	bal.

*Grain refiner, present as Al_6Mn in Al–Li–Mn and $Al_{20}Cu_2Mn_3$ in the Al–Cu–Li.
Note: No evidence of sodium or potassium in bulk analyses.

3. Materials and experimental procedure

The Al–Li–Mn alloy used in this research was produced by Alcoa Technical Center, Alcoa Center, Pennsylvania. The alloy was prepared by melting the aluminium and manganese under a salt flux of sodium chloride and lithium chloride. The lithium, sealed in high-purity vacuum cans, was inserted into the melt. The alloy was direct-chill (DC) cast, under a salt flux, as a 22.5 cm diameter and 45 cm long billet. The billet was preheated and extruded at 482° C in the form of hollow boxes with an extrusion ratio of 35 : 1.

The as-extruded Al–Li–Mn material was solution heat treated (SHT) in a molten salt bath for 15 min, cold-water quenched and immediately stretched for residual stress relief. The alloy was subsequently naturally aged for 3 days and refrigerated until needed. Ageing response at 171, 187 and 204° C was determined using an oil bath for hardness coupons of the SHT, quenched and naturally-aged material. Based on the hardness curves, an under-aged (4 h at 200° C), peak-aged (24 h at 200° C) and an over-aged condition (12 days at 200° C) were chosen for the study. The Al–Cu–Li alloy was received from the Air Force Materials Laboratory (AFML) as 25 mm thick rolled plate in the T651 condition, i.e. SHT, quenched, stress relieved and artificially aged to maximum hardness. The chemical compositions of the two alloys, in weight percent, are given in Table I and the processing treatment is summarized in Table II.

The samples for optical metallography were

TABLE II Heat-treatment schedule

Al–Li–Mn	Solution heat treated at 555° C ± 2° C for 15 min Cold-water quenched (CWQ) Room-temperature aged 3 days Stretched 1.5% Artificially aged at 200° C for (i) 4 h – under-aged (ii) 24 h – peak-aged (iii) 12 days – over-aged
Al–Cu–Li	Ingot cast and hot rolled to obtain 25 mm thick rolled plate Solution heat treated (SHT) at 516° C for 6 h Cold-water quenched (CWQ) Stretched 1.5 to 2.0% for residual stress relief Artificially aged at 160° C for 18 h to maximum hardness

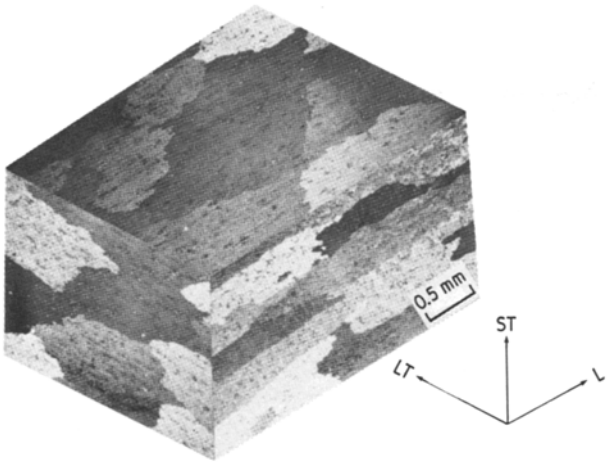

Figure 1 Triplanar optical micrograph illustrating the grain structure of the solution heat-treated Al–Li–Mn alloy.

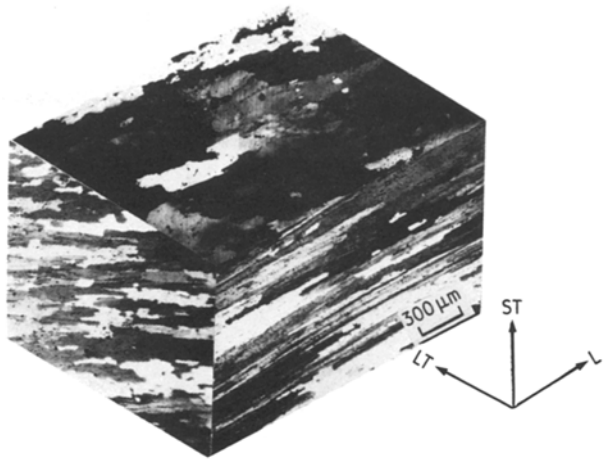

Figure 2 Triplanar optical micrograph illustrating the grain structure of the as-received Al–Cu–Li alloy, 2020–T651.

mounted, mechanically polished and etched by anodizing to reveal the high-angle grain boundaries. Optical micrographs of the longitudinal and long-transverse and short-transverse sections were taken using polarized light. In order to study the morphology and distribution of the dispersoids and constituent particles in the two alloy systems a bromine etch technique was used. The etched specimens were observed in a scanning electron microscope (SEM). Qualitative measurements of the various microstructural parameters were made by both manual and automated techniques. Fine microstructural features were revealed by transmission electron microscopy (TEM) using an operating voltage of 100 kV.

4. Results and discussion

4.1. Optical metallography

The microstructures of the experimental materials are shown in Figs. 1 and 2 as triplanar optical micrographs illustrating the grain structure of the material in the three orthogonal directions. The solution heat-treated Al–Li–Mn material, shown in Fig. 1, has primarily a recrystallized structure with large pancake-shaped grains. The grains are elongated parallel to the extrusion direction and have average grain dimensions of 2300 μm × 600 μm × 340 μm. The as-received, Al–Cu–Li alloy, produced by conventional processing, has a typical pancake-shaped grain structure with the grains flattened and elongated parallel to the rolling direction, Fig. 2. This material is partially recrystallized with a degree of recrystallization of 26% and average grain dimensions of 1000 μm × 500 μm × 125 μm.

Scanning electron microscopy studies of the bromine-etched samples of the Al–Li–Mn material revealed a bimodal distribution of Al_6Mn particles, as shown in Fig. 3a. The large particles up to 1 μm diameter form during solidification. The smaller particles, formed during heat treatment, are 0.3 μm diameter with an interparticle spacing of 5.5 μm and a volume fraction of 0.035 [11].

Numerous coarse secondary intermetallic particles

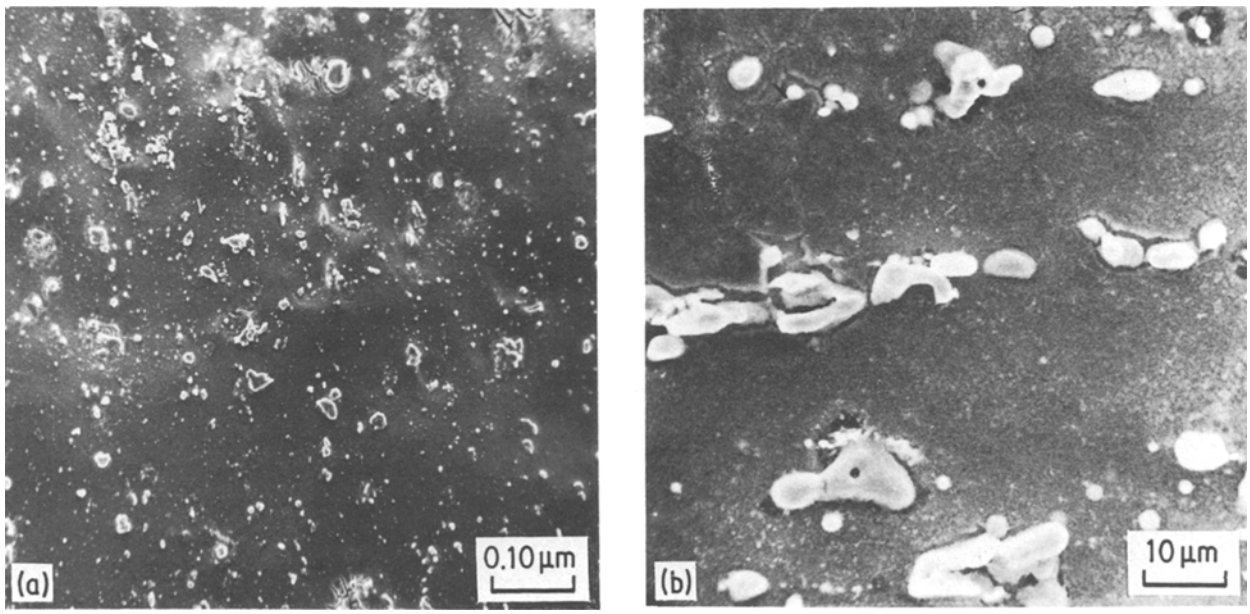

Figure 3 Scanning electron micrographs showing distribution of particles on bromine-etched surfaces of the experimental materials: (a) distribution of Al_6Mn in Al–Li–Mn, and (b) distribution of coarse Al_7Cu_2Fe, $Al_{12}(FeMn)_3Si$, and intermediate size $Al_{20}Cu_2Mn_3$ and Al_6Mn in Al–Cu–Li.

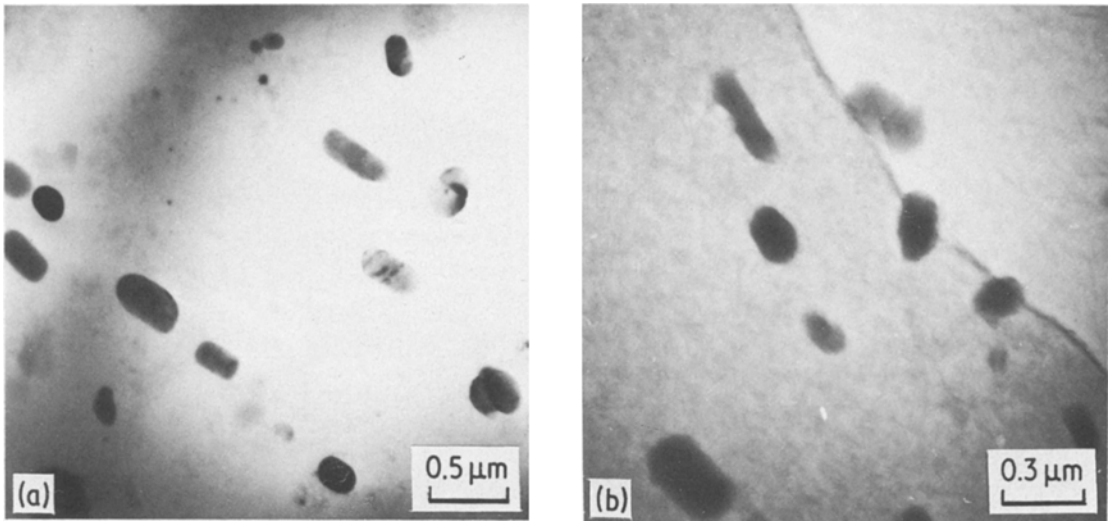

Figure 4 Bright-field transmission electron micrographs showing dispersoid particle distribution: (a) Al_6Mn particles in Al–Li–Mn, and (b) $Al_{20}Cu_2Mn_3$ and Al_6Mn in Al–Cu–Li.

were observed on the bromine-etched surfaces of the Al–Cu–Li material, as shown in Fig. 3b. These particles have been previously identified by electron microprobe and Guinier-de-Wolff X-ray diffraction method as compounds of Al_7Cu_2Fe, $Al_{12}(Fe\ Mn)_3Si$, $Al_{20}Cu_2Mn_3$ and Al_2CuLi [12]. The size of the coarse particles ranged from 1 to 10 μm in the longest dimension. In addition to coarse particles in the Al–Cu–Li alloy, smaller particles of the Al_6Mn type were also present. The particles ranged in size from 0.2 to 1 μm and are shown in Fig. 4.

The iron and silicon impurity elements in the ternary Al–Cu–Li material form large and intermediate size intermetallic particles which are difficult to eliminate by processing. The tendency for recrystallization to occur during processing is due to an inhomogeneous strain distribution which enhances the ability of the particles to act as favourable nucleation sites for recrystallization. In the Al–Cu–Li alloy system, some of the manganese is lost to the formation of the coarse constituent particle $Al_{12}(Fe\ Mn)_3Si$. The remaining manganese combines with both aluminium and copper to form incoherent dispersoids, $Al_{20}Cu_2Mn_3$ and Al_6Mn. The low volume fraction of the dispersoid particles is inadequate by itself to prevent recrystallization from occurring.

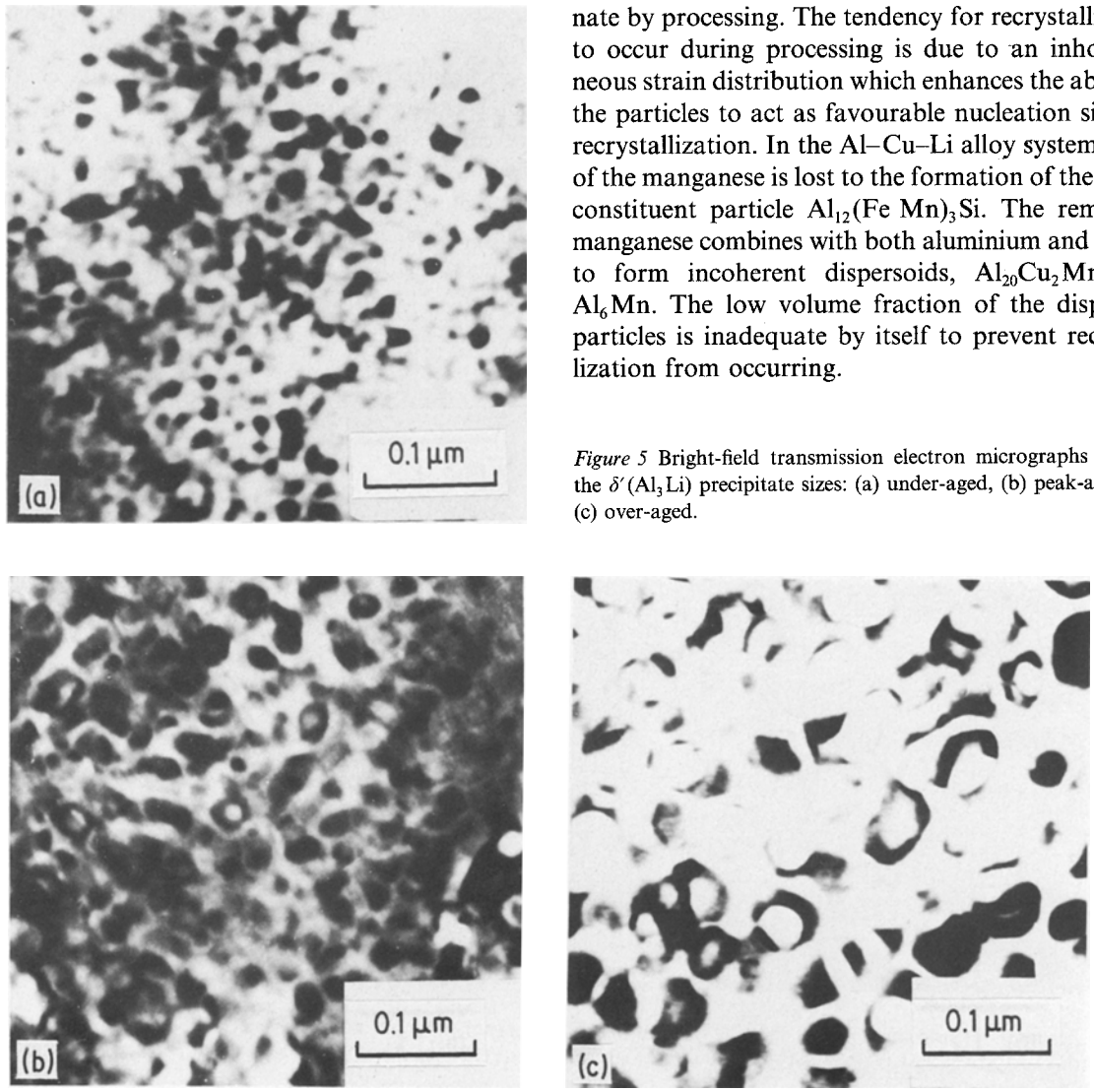

Figure 5 Bright-field transmission electron micrographs showing the $\delta'(Al_3Li)$ precipitate sizes: (a) under-aged, (b) peak-aged, and (c) over-aged.

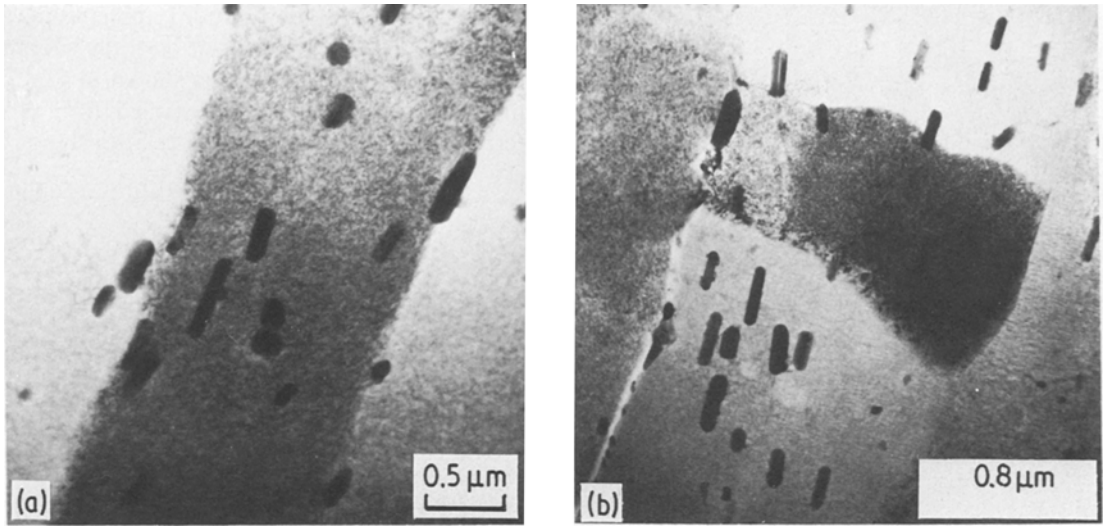

Figure 6 Bright-field transmission electron micrographs of Al–Cu–Li alloy showing: (a) large recrystallized grain with dispersed manganese containing dispersoids, and (b) subgrain structure within a large recrystallized grain.

The dispersoids in both the Al–Li–Mn and Al–Cu–Li alloys are aligned in the metal flow direction. This is a residual effect of the fabrication process generally referred to as "mechanical fibreing". The high volume fraction of secondary intermetallics present in the Al–Cu–Li alloy, due to the iron and silicon impurities, have the same preferred distribution as the dispersoids. During ingot solidification and subsequent processing these impurities combine with other elements and precipitate as insoluble constituent phases that cannot be taken into solution during subsequent heat treatment [13].

4.2. Transmission electron microscopy

Electron micrographs and selected-area diffraction (SAD) patterns revealed the fine scale microstructural details, e.g. subgrains, dispersoid particles and the morphology and nature of the strengthening precipitates. Some typical transmission electron micrographs, for the experimental materials, are shown in Figs. 5 to 11.

Transmission electron microscopic observations of the solution heat-treated Al–Li–Mn alloy for the under-aged, peak-aged, and the over-aged conditions revealed that the δ', Al_3Li, precipitate particles maintain a spherical shape throughout the ageing sequence studies. For the as-quenched and under-aged Al–Li–Mn alloy, there was no indication of the Guinier-Preston (GP) type precipitate that is observed in some age-hardenable, high-strength aluminium alloys. The bright-field electron micrographs of the δ' precipitate structure for the three ageing conditions are shown in Fig. 5. The sizes of the δ' precipitates in the under-aged, peak-aged and over-aged conditions were approximately 15, 30 and 75 nm in diameter, respectively. The grain-refining particles, Al_6Mn, were found to be present in both the interior of the grain and at the grain boundaries, as shown in Fig. 4.

Transmission electron microscope (TEM) observations of the Al–Cu–Li material revealed dispersoid particles, large recrystallized grains and sub-structures within unrecrystallized grains at low magnification, as

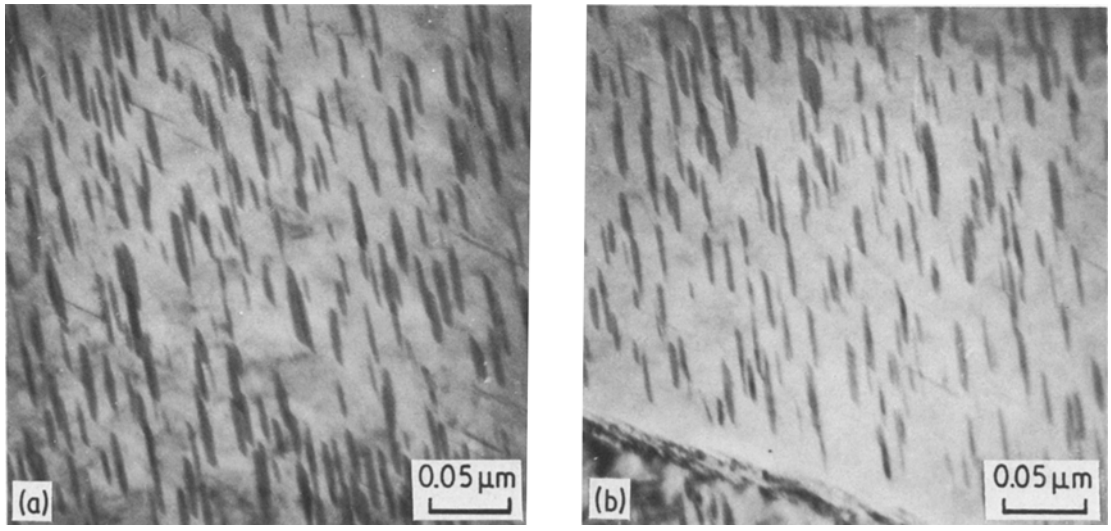

Figure 7 Bright-field transmission electron micrographs of Al–Cu–Li alloy showing needle-like nature of the Al–Cu precipitates: (a) within a large recrystallized grain, and (b) within a subgrain.

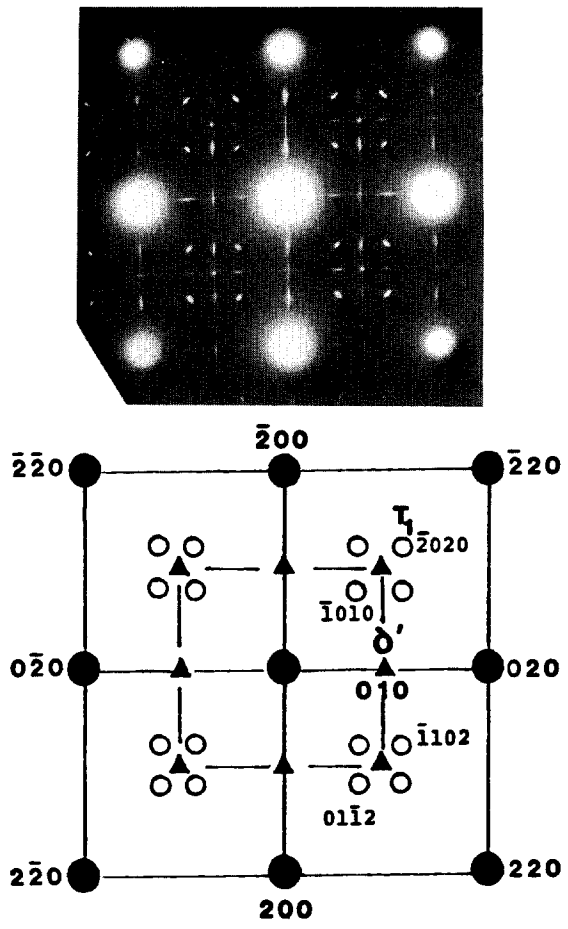

Figure 8 Selected-area diffraction pattern showing superlattice spots caused by the T_1 and δ' reflections. Zone axis: matrix (0 0 1); T_1 precipitate ($2\bar{4}23$).

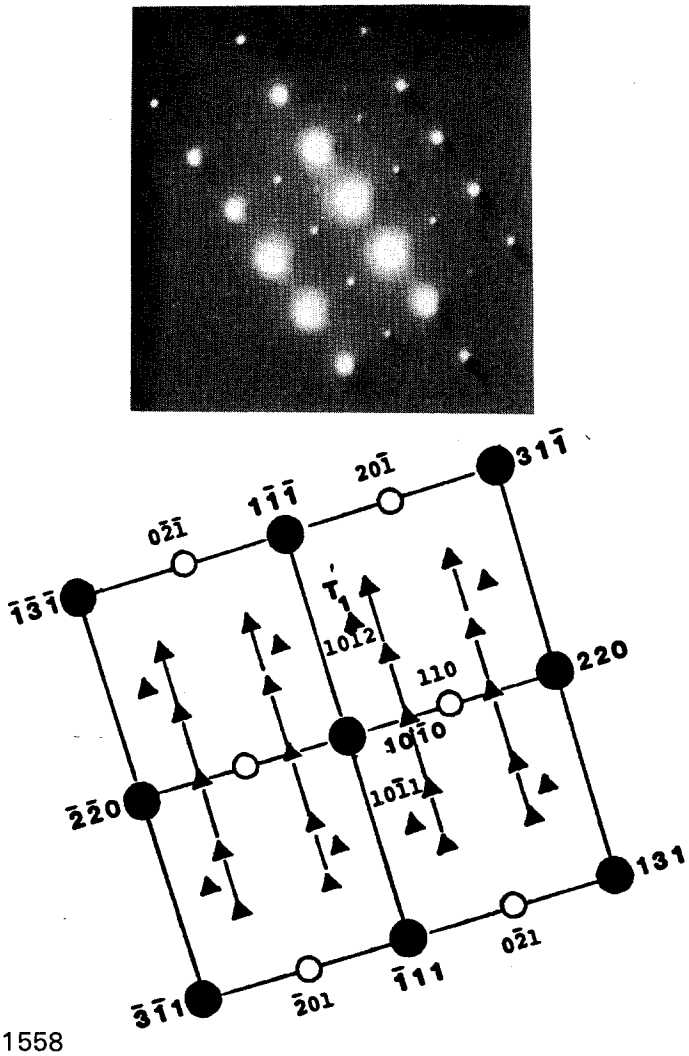

Figure 9 Selected-area diffraction pattern showing superlattice spots caused by the T_1 and δ' reflections. Zone axis: matrix ($1\,1\,\bar{2}$); T_1 ppt ($1\,1\,\bar{2}\,0$).

shown in Fig. 6. The θ' and T_1 precipitate particles were present in the interior of both the subgrains and large recrystallized grains, as shown in Fig. 7. These precipitate particles were identified from SAD patterns and have an orientation relationship [14]

$$[1\,0\,0]_{\text{matrix}} \parallel [1\,0\,0]_{\theta'} \quad \text{(Fig. 8)}$$

$$[2\,\bar{1}\,\bar{1}]_{\text{matrix}} \parallel [1\,1\,\bar{2}\,0]_{T_1} \quad \text{(Fig. 9)}$$

In the peak-aged condition, the θ' precipitate particles were significantly more prominent than either T_1 or T_B. The major strengthening precipitates in the peak-aged Al–Cu–Li alloy are coherent and partially coherent with the aluminium matrix.

The strengthening precipitates in the ternary Al–Cu–Li alloy were identified from SAD patterns. Fig. 8 shows a typical (1 0 0) electron diffraction pattern. The streaking parallel to the $\langle 1\,0\,0\rangle_{Al}$ and $\langle 0\,1\,0\rangle_{Al}$ was due to the plate-like θ' precipitates. Superlattice spots were also visible and were due to the ternary T_1 (Al_2CuLi) and binary δ' (Al_3Li) precipitate particles.

Precipitate-free zones were observed along the grain and subgrain boundaries in all three ageing conditions of the Al–Li–Mn alloy and along the interfaces of Al_6Mn particles scattered through the matrix. A PFZ for the peak-aged Al–Li–Mn alloy is shown in Fig. 10. The width of the PFZ increased with ageing. The sizes of the θ' precipitates and the widths of the PFZs for this alloy are summarized in Table III. In the Al–Cu–Li material, narrow PFZs, 0.05 μm wide, were observed along high-angle boundaries and at grain-boundary triple points, as shown in Fig. 11.

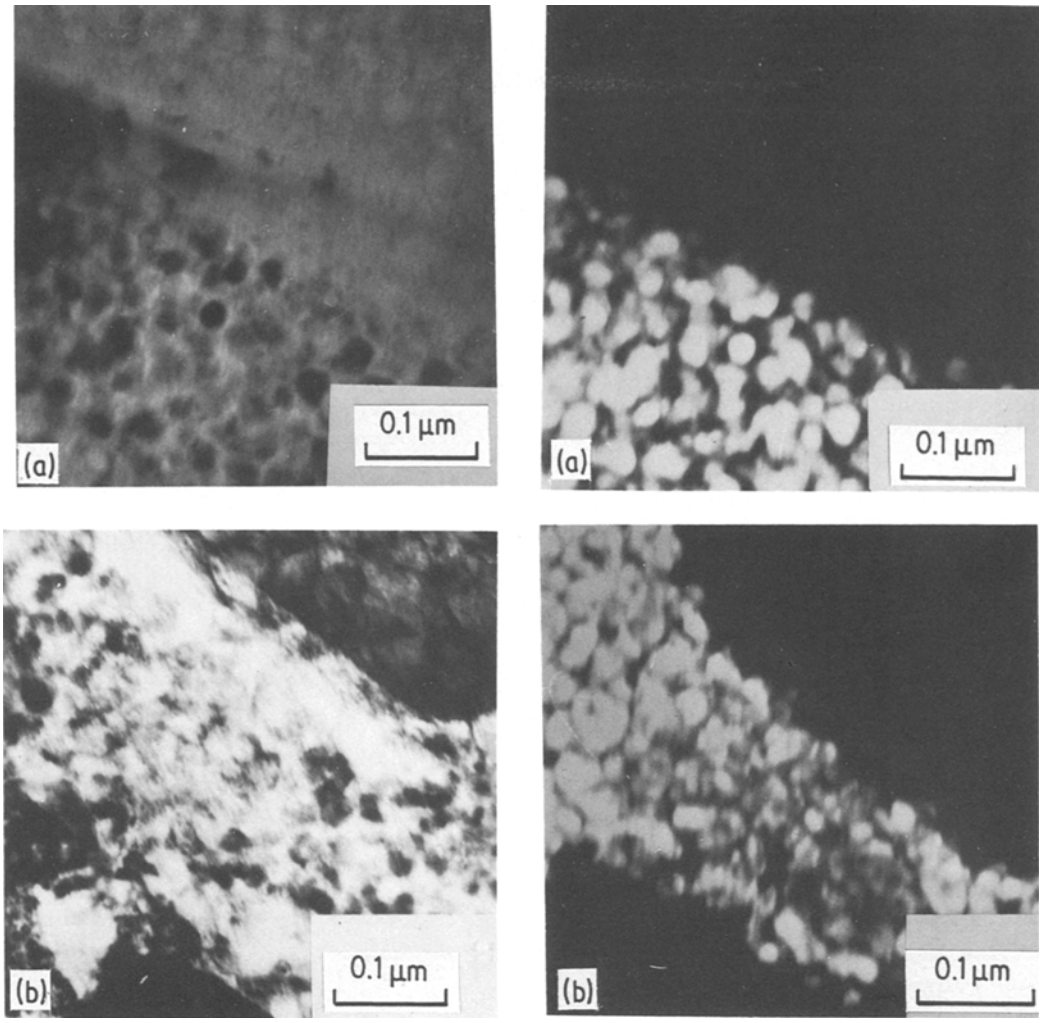

Figure 10 Transmission electron micrograph of Al–Li–Mn alloy showing: (a) bright-field (left) and dark-field (right) of PFZ at grain boundary, and (b) bright-field (left) and dark-field (right) of PFZ at Al_6Mn particles.

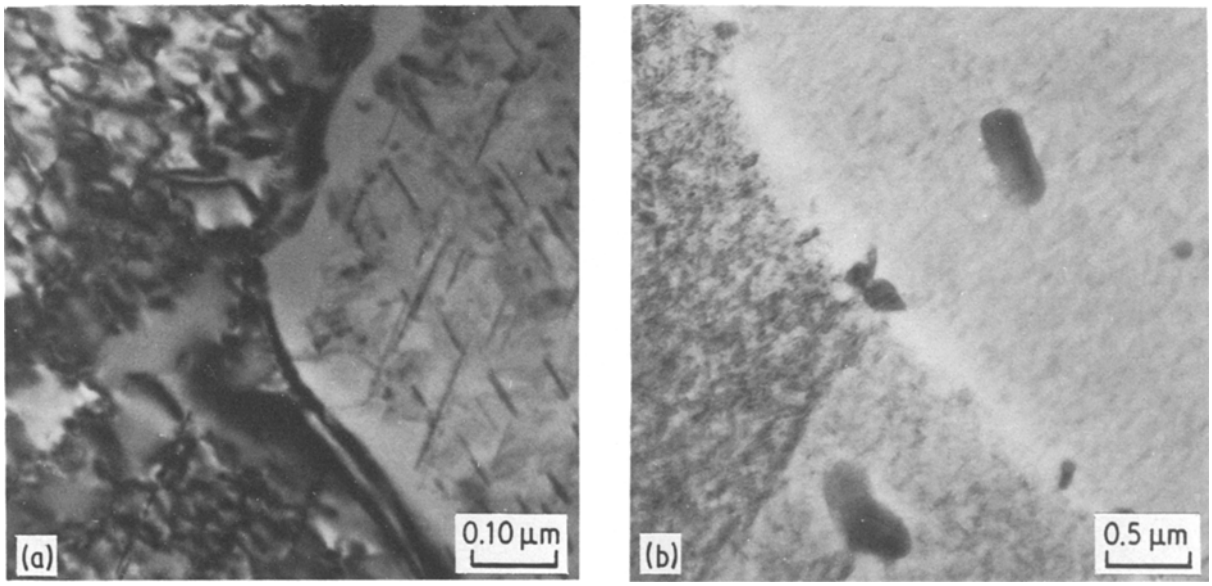

Figure 11 Bright-field transmission electron micrograph of peak-aged Al–Cu–Li alloy showing: (a) PFZ at grain boundary, and (b) PFZ at grain-boundary triple junction.

TABLE III Precipitate and PFZ sizes for Al–Li–Mn

Ageing condition	Precipitate size diameter (nm)	Precipitate spacing centre–centre (nm)	PFZ width
Under-aged	15	28	–
Peak-aged	30	56.5	700
Over-aged	75	141	–

Precipitate-free zones were, however, not found along the subgrain boundaries of this material.

5. Conclusions

1. Both the Al–Li–Mn and Al–Cu–Li alloy systems are partially recrystallized with large recrystallized grains.

2. The presence of iron and silicon impurities, in conjunction with the grain refiner manganese, results in a fairly high volume fraction of coarse intermetallic particles and intermediate size dispersoids.

3. Strengthening precipitates in the peak-aged Al–Cu–Li alloy and the under-aged and peak-aged Al–Li–Mn alloys, are fine, small in size, closely spaced and coherent or partially-coherent with the aluminium matrix. As ageing progresses beyond peak strength both particle size and interparticle spacing increases.

4. Precipitate-free zones are present in both the Al–Li–Mn and Al–Cu–Li alloy systems.

Acknowledgements

Dr E. J. Coyne Jr was supported by Lockheed-Georgia Company. Drs T. S. Srivatsan and E. A. Starke Jr were supported by the Air Force Office of Scientific Research under Grant AFOSR-78-3471, Dr Alan H. Rosenstein, Program Manager. The authors express thanks to both Lockheed-Georgia and Air Force for support of this research.

References

1. K. K. SANKARAN and N. J. GRANT, in Proceedings of the First International Conference on Aluminium-Lithium Alloys, Atlanta, Georgia, 1980, edited by T. H. Sanders Jr and E. A. Starke Jr (Metallurgical Society of AIME, Warrandale, Pennsylvania, 1981) pp. 205–27.
2. V. WIGOTSKY, *Aerospace Amer.* June (1984) 74.
3. J. M. SILCOCK, *J. Inst. Metals* **88** (1959–1960) 357.
4. B. NOBLE and G. E. THOMPSON, *Met. Sci. J.* **5** (1970) 114.
5. T. H. SANDERS Jr, E. A. LUDWICZAK and R. R. SAWTELL, *Mater. Sci. Eng.* **43** (1980) 247.
6. E. A. STARKE Jr and T. H. SANDERS Jr, *J. Metals* **33** (August) (1981) 24.
7. P. NISKANEN, T. H. SANDERS Jr, M. MAREK and J. G. RINKER, in Proceedings of the First International Conference on Aluminium-Lithium Alloys, Atlanta, Georgia, 1980, edited by T. H. Sanders Jr and E. A. Starke Jr (Metallurgical Society of AIME, Warrendale, Pennsylvania, 1981) pp. 347–76.
8. J. D. BOYD and R. B. NICHOLSON, *Acta Metall.* **19** (1971) 1379.
9. B. NOBLE and G. E. THOMPSON, *Met. Sci. J.* **6** (1972) 167.
10. F. S. LIN, S. B. CHAKRABORTTY and E. A. STARKE Jr, *Met. Trans. A* **13** (1982) 401.
11. E. J. COYNE Jr, PhD thesis, Georgia Institute of Technology (1979).
12. T. H. SANDERS Jr, Final Report, Naval Air Development Center, Warminister, Pennsylvania, Contract No. N62269-76-C-0271, Naval Air Systems Command (1979).
13. T. H. SANDERS Jr and J. T. STALEY, Review of Fatigue and Fracture Research on High Strength Aluminium Alloys, in "Fatigue and Microstructure", edited by M. Meshii (American Society for Metals, Metals Park, Ohio, 1979) pp. 467–516.
14. T. S. SRIVATSAN, PhD thesis, Georgia Institute of Technology (1984).

Received 23 January
and accepted 31 May 1985